On the nonlinear stability and detonability limit of a detonation wave for a model three-step chain-branching reaction

By MARK SHORT[1]† AND JAMES J. QUIRK[2]‡

[1]School of Mathematics, University of Bristol, Bristol BS8 1TW, UK

[2]Institute for Computer Applications in Science and Engineering, NASA Langley Research Center, Hampton, VA 23681-0001, USA

The nonlinear stability of a pulsating detonation wave driven by a three-step chain-branching reaction is studied. The reaction model consists sequentially of a chain-initiation step and a chain-branching step, both governed by Arrhenius kinetics, followed by a temperature-independent chain-termination step. The model mimics the essential dynamics of a real chain-branching chemical system, but is sufficiently idealized that a theoretical analysis of the instability is possible. We introduce as a bifurcation parameter the chain-branching cross-over temperature (T_B), which is the temperature at which the chain-branching and chain-termination rates are equal. In the steady detonation structure, this parameter controls the ratio of the chain-branching induction length to the length of the recombination zone. When T_B is at the lower end of the range studied, the steady detonation structure, which is dominated by the temperature-independent recombination zone, is found to be stable. Increasing T_B increases the length of the chain-branching induction region relative to the length of the recombination zone, and a critical value of T_B is reached where the detonation becomes unstable, with the detonation shock pressure evolving as a single-mode low-frequency pulsating oscillation. This single-mode nonlinear oscillation becomes progressively less stable as T_B is increased further, persisting as the long-term dynamical behaviour for a significant range of T_B before eventually undergoing a period-doubling bifurcation to a two-mode oscillation. Further increases in T_B lead to a chaotic behaviour, where the detonation shock pressure history consists of a sequence of substantive discontinuous jumps, followed by lower-amplitude continuous oscillations. Finally, for further increases in T_B a detonability limit is reached, where during the early onset of the detonation instability, the detonation shock temperature drops below the chain-branching cross-over temperature causing the wave to quench.

1. Introduction

Detonation waves are physico-chemical propagating structures that are composed of a lead shock wave which initiates chemical reaction in the reactive material. In

---

† Present address: Theoretical and Applied Mechanics, University of Illinois, Urbana, IL 61801, USA.

‡ Present address: Graduate Aeronautical Laboratories, Mail Code 205-45, California Institute of Technology, Pasadena CA 91125, USA.

turn, the release of chemical energy sustains the lead shock wave. The steady one-dimensional structure of a detonation wave was first determined independently by Zeldovich, Von-Neumann and Döring (Fickett & Davis 1979) and is known as the ZND structure. The minimum sustainable steady detonation speed is the Chapman–Jouguet (CJ) detonation velocity and is the speed at which the equilibrium or burnt zone flow is sonic relative to the lead shock wave. The presence of the sonic point causes a decoupling of the gasdynamic evolution of the equilibrium flow from the main detonation wave structure. Detonation waves travelling at speeds greater than CJ are called overdriven and have the property that the flow in the burnt region is subsonic relative to the detonation shock. Typical detonation speeds are of the order of 1000–2000 $\mathrm{m\,s^{-1}}$ in gases and 6000–8000 $\mathrm{m\,s^{-1}}$ in condensed solid explosives. Typical peak pressures are of the order of 20–100 atmospheres in gases and can reach upwards of a few hundred thousand atmospheres in condensed solid explosives (Fickett & Davis 1979).

In practice, stable one-dimensional detonation waves are seldom observed. Experimental investigations such as those of McVey & Toong (1971) and Alpert & Toong (1972) (see also the additional references contained in Abouseif & Toong 1982) describe a complex one-dimensional nonlinear pulsating detonation wave instability when blunt projectiles are fired into quiescent detonable mixtures. However, due to their complexity, the mechanisms underlying the pulsating instability are still poorly understood. Major difficulties include, for example, explaining why the pulsations can be either periodic or highly irregular depending on the nature of chemical mixture, and why the longitudinal density variations associated with the more irregular pulsations tend to be significantly larger than those associated with the regular pulsations.

Nevertheless, these studies serve to highlight a link between the nature of the pulsating detonation instability and its relation to the nature of the chemical reaction. This important link is the subject of our present study. Here, we present a comprehensive investigation of the nonlinear pulsating detonation instability for a one-dimensional detonation wave driven by a three-step reaction model. This model is specifically chosen to be representative of the actual dynamics of complex chain-branching chemistry. We include the results from both a linear stability analysis of the model system and a computational study for the fully nonlinear long-time evolution of the detonation instabilities. A detailed investigation into the hydrodynamic instability mechanism is left to a subsequent article.

To date, the majority of the theoretical work on one-dimensional detonation stability has been conducted for Arrhenius one-step reaction chemistry. The first formal linear stability studies were conducted by Erpenbeck (1962, 1964), who used a Laplace transform approach to analyse the behaviour of small-amplitude disturbances from the plane steady detonation wave. Later, Lee & Stewart (1990) formulated a normal mode approach, and their numerical shooting algorithm provided a significantly more straightforward technique for calculating the linear stability spectra. Within the Arrhenius model, the sensitivity of the chemistry to the hydrodynamic flow can be increased by increasing the activation energy associated with the reaction, and for a fixed detonation wave velocity this was found to destabilize the detonation.

In parallel with the linear stability analyses, there have been several studies concerned with the direct numerical simulation of the pulsating detonation instability driven by a one-step Arrhenius reaction. Using a characteristic technique and a finite difference technique respectively, Fickett & Wood (1964) and Abouseif & Toong (1982) were able to reproduce the salient stability predictions of Erpenbeck (1964). More recently, a significant improvement in the quality and

accuracy of such simulations was attained by Bourlioux, Majda & Roytburd (1991*a*). Using a finite-volume solution technique in conjunction with a simplified form of mesh refinement, they were able to obtain numerical results which are in close agreement with the theoretical predictions of Lee & Stewart (1990). However, even the latter studies of Bourlioux *et al.* (1991*a*) did not explore the very long-time propagation behaviour and so in many cases the actual nonlinear dynamical behaviour for the one-step Arrhenius pulsating detonation instability remains undetermined.

In practice, a large class of chemical reactions are not represented effectively by a one-step Arrhenius reaction model. Rather, a large majority of chemical reactions are chain branching and proceed by a sequence of chain-initiation, chain-branching and chain-termination stages. Typically in such reactions, a small amount of the reactant is converted into chain carriers, which may be either free radicals or atoms, by means of relatively slow initiation reactions. These chain carriers are then rapidly multiplied through a sequence of self-accelerating chain-branching reactions, while the rise in concentration of radicals is retarded by termination steps which occur either through absorption at the vessel walls or through three-body collisions in the interior. We recognize that due to the different temperature sensitivities of a chain-branching chemical reaction over a one-step Arrhenius reaction, the inherent stability characteristics of a detonation wave in each case are likely to be markedly different.

To the authors' knowledge, there has only been one previous theoretical study which specifically recognizes the important differences between chain-branching reaction mechanisms and an Arrhenius one-step thermal-decomposition model in relation to the pulsating detonation instability problem. Fickett, Jacobson & Schott (1972) introduced a simple one-step representation of a chain-branching kinetic model which they described as a "mock-up". However, this model could be tuned to cover two possible reaction zone structures in the initial steady detonation wave: the first is one in which the exothermic reaction zone is much longer than the induction zone and the second is one in which the reaction zone is of the same order of length as the induction zone. The former regime was claimed to be representative of a hydrogen–oxygen–diluent system, namely $2H_2 + O_2 + 9Ar$, at an initial low pressure of 0.1 atm and temperature 300 K. The second regime was stated to be representative of the same hydrogen–oxygen–diluent reaction but at higher initial pressures. Additionally, it was proposed that the second regime might also be appropriate for some unsaturated hydrocarbon–oxygen reactions. Fickett *et al.* (1972) presented the results of full numerical simulations of a pulsating instability associated with both reaction zone structures. However, as noted by Abouseif & Toong (1982), it is difficult to gain any quantitative insight regarding the improvement of this chain-branching model over the one-step Arrhenius model, since no linear stability analysis was conducted in parallel to the computational study.

For the present theoretical study we employ a three-step reaction model, also presented in Short & Dold (1996), based on a generalization of model of Gray & Yang (1965) in order to conduct a carefully controlled study into the behaviour of a pulsating detonation wave driven by a chain-branching reaction. This model contains a chain-initiation step in which an energetically difficult Arrhenius reaction produces a small concentration of chain carriers from the reactant. A lower-activation-energy chain-branching reaction step, which is also of Arrhenius type, then leads to an acceleration in the concentration of chain carriers. The final component of the model is an exothermic termination reaction in which chain carriers are converted into products independently of temperature. Although this model falls short of full

reaction kinetics, in contrast to the classical one-step Arrhenius model it does retain the essential chemical dynamics of a real chain-branching reaction.

A crucially important parameter within our chosen reaction model is the value of the chain-branching cross-over temperature, T_B, which is the temperature at which the chain-branching and chain-termination rates are equal. Later on in this paper we shall demonstrate that depending on the value of T_B, there are three possible limiting profiles for the spatial structure of a steady detonation wave; the chain-branching induction zone is either much shorter than, of the same order as, or significantly longer than the length of the recombination zone. As noted by Fickett *et al.* (1972), such changes in the underlying steady detonation profile can be attributed to either changes in the chemical composition of the detonable mixture or changes in its initial pressure. Several experimental investigations, summarized in Strehlow (1970) and Lee (1984), detail the importance of the relative size of the recombination zone to induction zone in relation to the properties of detonation wave propagation. This is so since the stability characteristics of the detonation wave are markedly different in each of the three limiting cases. Consequently, we have chosen to use the chain-branching cross-over temperature T_B as a bifurcation parameter in our linear and nonlinear stability investigation.

The rest of the paper is as follows. In the next section we present the model we have used for our investigation and describe the modelling assumptions behind it. In §3 we detail the spatial structure of the steady detonation wave admitted by the model, and describe how this structure varies as the bifurcation parameter T_B is varied. In §4, we present an analysis which determines an order of magnitude estimate for the chain-branching induction length given the instantaneous shock temperature. Then, in §5 we present the results from a linear stability analysis of the model system. This is followed by a section which outlines the numerical techniques we have used to obtain the direct numerical simulations of the nonlinear evolution of the pulsating one-dimensional detonation instabilities. The results from this computational study are discussed in §7. Finally, in §8 we end this paper with some conclusions that we have drawn from our investigation.

2. Model

The hydrodynamic behaviour of the fluid is modelled with the compressible one-dimensional reactive Euler equations which can be written in non-dimensional form as

$$\frac{\mathrm{D}\rho}{\mathrm{D}t} + \rho \frac{\partial u}{\partial x^l} = 0, \quad \frac{\mathrm{D}u}{\mathrm{D}t} + \rho^{-1} \frac{\partial p}{\partial x^l} = 0, \quad \frac{\mathrm{D}e}{\mathrm{D}t} + p \frac{\mathrm{D}\rho^{-1}}{\mathrm{D}t} = 0. \tag{2.1}$$

The variables ρ, u, p and e are the density, velocity, pressure and specific internal energy respectively. The substantive derivative

$$\frac{\mathrm{D}}{\mathrm{D}t} = \frac{\partial}{\partial t} + u \frac{\partial}{\partial x^l}, \tag{2.2}$$
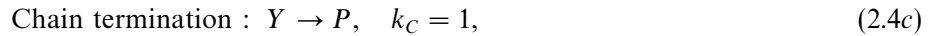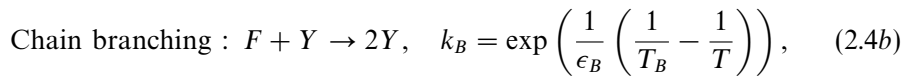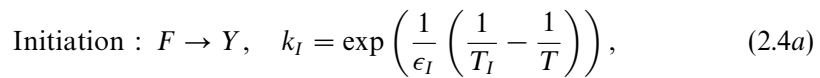
contains the usual partial derivatives in time t, and Cartesian laboratory-coordinate space x^l. We assume a polytropic equation of state and an ideal thermal equation of state, such that

$$e = \frac{p}{(\gamma - 1)\rho} - q, \quad T = p/\rho, \tag{2.3}$$

where q represents the local chemical heat energy, γ is the ratio of specific heats and T is the temperature. These equations admit a steady wave solution (§3) which is used

to provide non-dimensional scales for the density, pressure, temperature and velocity as the post-shock density, pressure, temperature and sound speed respectively. The scalings for length and time are determined below.

Based on the chain-branching reaction model of Gray & Yang (1965) and the later generalized reaction models, e.g. those described in Williams (1985), Strehlow (1986) and Griffiths & Barnard (1995), we assume that the essential dynamics of a global chain-branching reaction can be represented by three main stages: chain initiation, chain branching and chain termination with rate constants k_I, k_B and k_C respectively. On this basis, a model for a global chain-branching reaction can be represented via the following three primary reaction stages:

$$\text{Initiation}: \quad F \rightarrow Y, \quad k_I = \exp\left(\frac{1}{\epsilon_I}\left(\frac{1}{T_I} - \frac{1}{T}\right)\right), \qquad (2.4a)$$

$$\text{Chain branching}: \quad F + Y \rightarrow 2Y, \quad k_B = \exp\left(\frac{1}{\epsilon_B}\left(\frac{1}{T_B} - \frac{1}{T}\right)\right), \quad (2.4b)$$

$$\text{Chain termination}: \quad Y \rightarrow P, \quad k_C = 1, \qquad (2.4c)$$

for fuel F, chain radicals Y and product P. With reference to the reaction dynamics of a number of real chain-branching reactions (see for example Strehlow 1986), the following assumptions have been made regarding the model reaction mechanism. The chain-initiation and chain-branching rate constants k_I and k_B are taken to have Arrhenius temperature-dependent form with inverse activation energies ϵ_I and ϵ_B respectively. The chain-termination reaction is assumed to be first order, independent of temperature and is modelled as having a fixed rate constant. For our purposes, the reaction model (2.4) is the simplest realistic mechanism which reproduces the actual dynamics of a chain-branching reaction. Generalizations such as higher-order chain-termination reactions could also be considered in order to further improve the model, but this is not our concern at present. Kapila (1978) has used a similar model to study the homogeneous explosion problem for a chain-branching reaction in the limit of high activation energies, while Dold & Kapila (1991) consider the evolution of a shock-perturbed atmosphere.

The reference time t_c is scaled such that the chain-termination rate constant is unity, i.e. $k_C = 1$, with the reference length set to t_c times the sound speed immediately behind the detonation shock. Thus all length and time scales are based on ratios of the recombination time and length. The remaining parameters in (2.4) to be defined are T_I and T_B, which represent the respective cross-over temperatures at which the chain-initiation and chain-branching rates become as fast as the chain-termination rate. Consumption equations for fuel and radical then become

$$\frac{\mathrm{D}f}{\mathrm{D}t} = -r_I - r_B, \quad \frac{\mathrm{D}y}{\mathrm{D}t} = r_I + r_B - r_C, \qquad (2.5a,b)$$

where

$$r_I = f \exp\left(\frac{1}{\epsilon_I}\left(\frac{1}{T_I} - \frac{1}{T}\right)\right), \quad r_B = \rho f y \exp\left(\frac{1}{\epsilon_B}\left(\frac{1}{T_B} - \frac{1}{T}\right)\right), \quad r_C = y, \quad (2.6)$$

and f and y are the mass fractions of fuel and radical respectively. Finally the chemical energy q is defined as

$$q = Q - Qf - (Q + R)y, \qquad (2.7)$$

where $Q > 0$ represents the total chemical energy available in the unreacted mixture

and R represents the amount of endothermic energy absorbed by the initiation and chain-branching reactions in breaking down the reactant F into the energetic radical Y.

Also, in typical chain-branching reactions the chain-initiation reactions are energetically inhibited, as unimolecular dissociation reactions tend to have an activation energy greater than the bond dissociation energy (Griffiths & Barnard 1995). Although bimolecular initiation reactions tend to have lower activation energies, they also have lower pre-exponential factors and so are not significantly faster than unimolecular dissociation reactions. Therefore, given a steady post-shock detonation temperature of unity with the present scalings, we set

$$T_I > 1, \quad \epsilon_I \ll 1, \tag{2.8}$$

in order to mimic this behaviour. The chain-branching reactions, on the other hand, have a lower activation energy involving reactions between energetic free radicals or atoms and a rapid reaction rate once a sufficient concentration of chain radicals is established. Therefore, we set,

$$T_B < 1, \quad \epsilon_I \ll \epsilon_B \ll 1. \tag{2.9}$$

Finally it is well established that a number of chain-branching reactions, e.g. that of a hydrogen–air reaction, liberate only a small amount of chemical heat energy during the initiation and branching stages. For the purposes of the present paper, it is thus assumed that the chain-initiation and chain-branching steps in (2.4) are thermally neutral, i.e. we take

$$R = 0. \tag{2.10}$$

3. Steady detonation structure

The present flow model admits a steady one-dimensional detonation wave solution, denoted in the following by the superscript *, whose structure can be determined through the Rankine–Hugoniot relations. Assuming the steady detonation to propagate to the left along the path $x^l = -D_s^* t$, where D_s^* is the steady detonation Mach number relative to the post-shock sound speed, and denoting the detonation Mach number relative to the upstream unreacted material by D^*, the pressure, velocity and density satisfy

$$p^* = a + (1-a)\left(1 - bq^*\right)^{1/2}, \quad u^* = \frac{1-p^*}{\gamma M_s^*} + M_s^*, \quad \rho^* = \frac{M_s^*}{u^*}, \tag{3.1}$$

in the steady shock-attached coordinate system

$$X = x^l + D_s^* t, \tag{3.2}$$

where

$$M_s^{*2} = \frac{(\gamma-1)D^{*2}+2}{2\gamma D^{*2}-(\gamma-1)}, \quad a = \frac{\gamma M_s^{*2}+1}{(\gamma+1)}, \quad b = \frac{M_s^{*2}2\gamma(\gamma-1)}{(1-a)^2(\gamma+1)}. \tag{3.3}$$

These relations are independent of the functional form of the energy release q^*. Here, q^* satisfies

$$q^* = Q - Qf^* - Qy^*. \tag{3.4}$$

The variation in fuel and radical concentrations are determined by the first-order equations

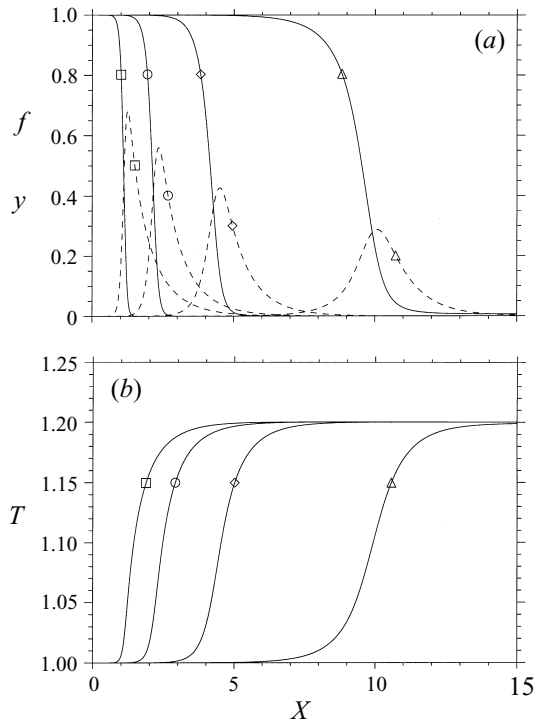$$f_{,X}^* = -(r_I^* + r_B^*)/u^*, \quad y_{,X}^* = (r_I^* + r_B^* - r_C^*)/u^*. \tag{3.5}$$

FIGURE 1. Steady detonation profiles showing (*a*) fuel, f, (solid lines) and radical, y, (dashed lines) and (*b*) temperature T. The symbols mark corresponding profiles for chain-branching cross-over temperatures $T_B = 0.80$ (□), $T_B = 0.85$ (○), $T_B = 0.90$ (◇) and $T_B = 0.95$ (△).

Given that the steady variables satisfy the shock conditions,

$$\rho^* = p^* = T^* = 1, \quad u^* = M_s^*, \quad f^* = 1, \quad y^* = 0, \tag{3.6}$$

the relations (3.5) may be integrated away from the shock at $X = 0$ so as to determine the complete structure of the steady detonation wave for $X > 0$. The detonation velocity D^* is determined by specification of the detonation overdrive, d, defined by

$$d = \left(\frac{D^*}{D_{CJ}^*}\right)^2 \tag{3.7}$$

where D_{CJ}^* is the Chapman–Jouguet detonation velocity, i.e. the minimum sustainable detonation velocity determined by the velocity being exactly sonic $u^* = (p^*/\rho^*)^{1/2}$ at the end of the wave where $q^* = Q$. We note that under the assumptions (2.8) and (2.9) the following ordering of the rate constants holds at the detonation shock:

$$k_I \ll k_C = 1 \ll k_B, \tag{3.8}$$

where the chain-initiation rate constant is exponentially small and the chain-branching rate constant is exponentially large. However, since $y^* = 0$ at $X = 0$, the concentration of chain radicals can only grow initially at the exponentially small rate k_I.

Figure 1 shows the variation in the steady detonation structure as T_B varies from $T_B = 0.8$ to $T_B = 0.95$ in steps of 0.05 holding the following parameters fixed: $Q = 3$, $R = 0$, $\epsilon_I = 1/20$, $\epsilon_B = 1/8$, $T_I = 3$, $\gamma = 1.2$, $d = 1.2$. Figure 1(*a*) shows profiles for fuel f and radical y as a function of the distance behind the detonation

shock, while figure 1(*b*) shows the corresponding variation in the temperature T. For the lower values of T_B, there is a short chain-branching induction zone with a significant build up in concentration of chain radicals behind the detonation shock. The chain-termination region is much longer than the chain-branching induction zone. This arises due to the fact that for the lower T_B, the rate of the chain-branching reaction is significantly greater than that of the termination reaction, which only becomes dominant after most of the fuel has been depleted. As T_B increases, the chain-branching induction zone becomes longer, and the peak concentration of chain radicals drops. For the higher T_B, the detonation structure is dominated by a long chain-branching induction zone, with only a moderate peak concentration of chain radicals being established. Here, the lower rate of the chain-branching reaction allows the chain-termination reaction to become effective before all the fuel is depleted, thus restricting the rise in concentration of chain radicals.

4. Quasi-steady estimates of the chain-branching induction length

We now obtain an order of magnitude estimate for both the chain-branching induction length in the steady detonation wave profiles above and the possible changes in chain-branching induction length which can occur during the propagation of an unstable detonation. These estimates are constructed under the assumption of a quasi-steady auto-ignition model in which the length of the chain-branching induction zone depends only on the shock state. Such auto-ignition solutions are valid in the limit of very slowly varying detonation structures. Under this assumption, the build up of chain radicals in the induction zone is governed by the asymptotic equations

$$\left. \begin{array}{ll} M_s y_X = k_I + k_B y & \text{if } k_B \gg 1, \quad T_s > T_B, \\ M_s y_X = k_I & \text{if } k_B = 1, \quad T_s = T_B, \end{array} \right\} \tag{4.1}$$

where M_s is the instantaneous post-shock fluid velocity corresponding to the instantaneous post-shock temperature T_s, and

$$k_I = \exp\left(\frac{1}{\epsilon_I}\left(\frac{1}{T_I} - \frac{1}{T_s}\right)\right), \quad k_B = \exp\left(\frac{1}{\epsilon_B}\left(\frac{1}{T_B} - \frac{1}{T_s}\right)\right). \tag{4.2}$$

Equations (4.1) have the solution

$$\left. \begin{array}{ll} y = \dfrac{k_I}{k_B}\left(e^{(k_B/M_s)X} - 1\right) & \text{if } k_B \gg 1, \\[2mm] y = \dfrac{k_I}{M_s}X & \text{if } k_B = 1. \end{array} \right\} \tag{4.3}$$

Assuming that $T_B < 1$, it can be determined from (4.3) that in order for the chain-branching induction length, i.e. the distance behind the shock where y becomes $O(1)$, to be of the same order as the recombination length, i.e. the distance from the main reaction to where all the radical is consumed, we require the following ordering in k_I and k_B to hold:

$$k_I = O(k_B e^{-k_B/M_s}). \tag{4.4}$$

Alternatively, the chain-branching induction length will be either much smaller or much larger than the recombination length depending on whether

$$k_I \gg k_B e^{-k_B/M_s} \quad \text{or} \quad k_I \ll k_B e^{-k_B/M_s}, \tag{4.5}$$

respectively.

For the steady detonation wave above, where $T_s = 1$, the first inequality is satisfied for lower values of T_B, i.e. higher values of k_B, than the second inequality. Consequently, this behaviour indicates that as T_B is increased from some lower value less than 1, e.g. $T_B = 0.8$ where the chain-branching induction length is initially much smaller than the chain-recombination length, the chain-branching induction length will eventually become much larger than the recombination length due solely to the increase in T_B. Moreover, for a fixed value of T_B but varying T_s, an interchange between the inequalities in equation (4.5) can readily occur. Finally, we note that for a fixed value of T_B, a special case arises when $T_s = T_B$. Under this circumstance, $k_B = 1$, and the chain-branching induction length is governed by the second of (4.3) and found to be of size $O(k_I^{-1})$. Thus the reaction zone is found to lie an exponentially large distance from the detonation shock, indicting a detonability limit has been reached. Examples showing the failure of the detonation when the shock temperature drops to the chain-branching temperature are shown in §7.

5. Linear stability results

A normal mode linear stability analysis has been conducted for the steady detonation wave structure (3.1)–(3.5) with the model chain-branching reaction scheme (2.4) as the bifurcation parameter T_B is varied. This proceeds by defining a shock-attached co-ordinate system,

$$x = X - \psi(t), \tag{5.1}$$

where $\psi(t)$ represents the perturbation to the steady shock location. Perturbations to the steady detonation structure are then sought in the form,

$$z = z^*(x) + z'(x)e^{\alpha t}, \quad \psi = \psi' e^{\alpha t}, \tag{5.2}$$

where

$$z = [v, \ u, \ p, \ f, \ y]^T, \tag{5.3}$$

$v = 1/\rho$ is the specific volume, $\mathrm{Re}(\alpha)$ is the disturbance growth rate and $\mathrm{Im}(\alpha)$ the disturbance frequency. Substituting (5.1) and (5.2) into (2.1)–(2.6) results in a system of first-order linear differential equations for the vector of complex perturbation eigenfunctions $z'(x)$. This system can be written in the form

$$\alpha z' + A^* z'_{,x} + C^* z' - \alpha b^* = 0, \quad b^* = z^*_{,x}, \tag{5.4}$$

where $z'(x)$ is renormalized such that $z'/\psi' \mapsto z'$, and where

$$A^* = \begin{pmatrix} u & -v & 0 & 0 & 0 \\ 0 & u & v/\gamma & 0 & 0 \\ 0 & \gamma p & u & 0 & 0 \\ 0 & 0 & 0 & u & 0 \\ 0 & 0 & 0 & 0 & u \end{pmatrix}^*, \quad C^* = \begin{pmatrix} -u_{,x} & v_{,x} & 0 & 0 & 0 \\ p_{,x}/\gamma & u_{,x} & 0 & 0 & 0 \\ -\alpha_v & p_{,x} & \gamma u_{,x} & 0 & -\alpha_y \\ \beta_v & f_{,x} & \beta_p & \beta_f & \beta_y \\ -\beta_v & y_{,x} & -\beta_p & -\beta_f & -\beta_y + 1 \end{pmatrix}^*. \tag{5.5}$$

The undefined quantities in C^* are

$$\beta_v = \frac{r_I}{\epsilon_I v T} + \frac{r_B}{\epsilon_B v T} - \frac{r_B}{v}, \quad \beta_p = \frac{r_I}{\epsilon_I p T} + \frac{r_B}{\epsilon_B p T}, \quad \beta_f = \frac{r_I}{f} + \frac{r_B}{f}, \quad \beta_y = \frac{r_B}{y}, \tag{5.6}$$

and

$$\alpha_v = -\frac{(\gamma - 1)}{v^2}Qy, \quad \alpha_y = \frac{(\gamma - 1)}{v}Q. \tag{5.7}$$

The perturbation shock conditions are determined from the Rankine–Hugoniot conditions as

$$v' = \frac{4\alpha}{(\gamma + 1)D^{*2}M_s^*}, \quad u' = \frac{2(1 + D^{*2})\alpha}{(\gamma + 1)D^{*2}}, \quad p' = -\frac{4\gamma M_s^*\alpha}{(\gamma + 1)}, \quad f' = 0, \quad y' = 0. \tag{5.8}$$

Finally, we apply a boundary condition in the burnt zone of the detonation wave such that there are no acoustic waves propagating upstream from infinity. This leads to the standard acoustic radiation condition in inert flows,

$$u' - \frac{v_b^*}{\gamma c_b^*}p' = 0 \tag{5.9}$$

where v_b^* and c_b^* are the unperturbed specific volume and isentropic sound speed in the burnt gas. This condition is applied at $x = \infty$, i.e. at the equilibrium point of the detonation for the present reaction model, where $f^* = y^* = 0 +$ exponentially small terms.

For a given set of initial thermodynamic and chemical parameters characterizing the steady detonation structure, the complex eigenvalues α and eigenfunctions $z'(x)$ are determined by a numerical shooting technique based on that of Lee & Stewart (1990). This involves taking an initial guess for α, integrating (5.4) from the perturbed shock conditions (5.8) into the burnt zone, and iterating on the initial guess until the acoustic radiation condition (5.9) is satisfied in the burnt zone at a point where the perturbation eigenfunctions of the exponentially decaying reaction terms are negligibly small relative to the terms present in (5.9).

Figure 2 shows the linear stability behaviour as the bifurcation parameter T_B is varied with the following thermodynamic and chemical parameters fixed: $Q = 3$, $R = 0$, $\epsilon_I = 1/20$, $\epsilon_B = 1/8$, $T_I = 3$, $\gamma = 1.2$, $d = 1.2$. Figure 2(a) shows the migration of the growth rate $\mathrm{Re}(\alpha)$ of the first nine unstable modes as the chain-branching cross-over temperature T_B is increased in the range $T_B \in [0.8, 1.0]$. Figure 2(b) shows the corresponding migration of the frequency $\mathrm{Im}(\alpha)$ of each mode with T_B. The steady detonation wave is stable to small disturbances for $T_B < 0.803$. In this range, the underlying steady detonation wave profile is dominated by the chain-termination region (figure 1). As the chain-termination reaction is independent of temperature, we note a relation to the work of Erpenbeck (1965), who considered the stability properties of a detonation wave with an idealized one-step reaction model having a zero activation energy. It was found that with such reaction models, the detonation wave has a greater tendency towards stability than with a chemical model with temperature-dependent reaction kinetics.

At $T_B = 0.803$, a neutrally stable mode appears. This mode has a low-frequency of oscillation with $\mathrm{Im}(\alpha) = 0.219$ and period $\Omega = 28.69$. As T_B increases through $T_B = 0.803$, a Hopf bifurcation occurs, rendering the detonation linearly unstable to the low-frequency disturbance. At $T_B = 0.821$, a second unstable mode appears having a much larger frequency than the first. As T_B increases further, additional unstable roots appear each having a progressively higher frequency than the previous root. This behaviour corresponds to an increase in the length of the temperature-dependent chain-branching induction length with increasing T_B. Table 1 gives the exact values of the growth rates and periods for the most unstable roots with increasing T_B. However, it is seen from both figure 2(a) and table 1 that the fastest growing mode
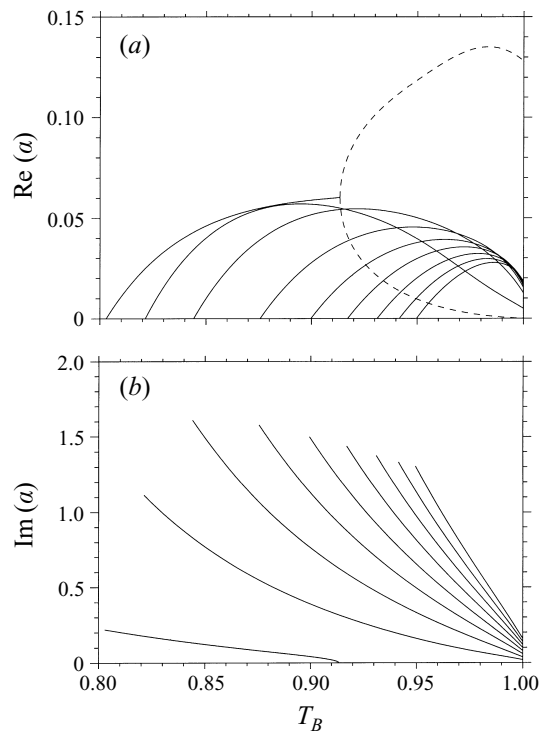
FIGURE 2. The variation in (*a*) the growth rate Re(α) and (*b*) the frequency Im(α) of one-dimensional instabilities as T_B is varied. The first nine unstable roots for increasing T_B are plotted. Purely real roots are shown as dashed lines.

for any value of T_B is always the fundamental low-frequency mode α_1. As T_B increases the frequency of this mode diminishes, until at $T_B = 0.913$ the low-frequency mode undergoes a pitchfork bifurcation into two non-oscillatory modes having an infinite period. One branch of the root has a growth rate which continues to increase with T_B, while the other has a growth rate which decays with T_B, with Re(α) $\to 0$ at $T_B = 1$. Corresponding to an increase in T_B, the reaction zone in the steady structure lies progressively further downstream of the shock, and thus the propagation time for acoustic disturbances between the shock and flame increases. The steady structure then resembles that of a flat-top inert shock, followed a long way downstream by a decoupled fast-flame reaction zone structure. Pulsating modes of instability arise from acoustic waves periodically reflecting between the shock and reaction zone. However, if they are sufficiently decoupled, then the stability is determined by the inherent stability of both structures independently. For an ideal gas, the shock front is stable or neutrally stable, while initial calculations show that in an unbounded atmosphere, the fast flame possesses only purely real modes of low-frequency instability (Short & Clarke 1997).

The bifurcation of the low-frequency modes into two non-oscillatory modes is also of interest in light of two recent studies into detonation stability by He & Lee (1995) and Short (1997). These authors observed similar bifurcations in the linear stability spectra arising from a one-step Arrhenius reaction as the overdrive is decreased (He & Lee 1995), as the activation energy is increased, or in two dimensions, the wavenumber is increased (Short 1997). He & Lee (1995) also suggest that the point

T_B	n	$\text{Re}(\alpha) \times 10^{-2}$	$\pm\text{Im}(\alpha)$	Ω
0.790	α_1	−2.572	0.2520	24.93
	α_2	−9.782	1.6675	3.77
0.800	α_1	−0.501	0.2265	27.74
	α_2	−5.800	1.4646	4.29
0.805	α_1	0.355	0.2144	29.31
	α_2	−4.147	1.3731	4.58
0.820	α_1	2.354	0.1804	34.83
	α_2	−0.276	1.1327	5.55
0.830	α_1	3.316	0.1597	39.34
	α_2	1.576	0.9966	6.30
0.840	α_1	4.054	0.1404	44.75
	α_2	2.976	0.8766	7.17
0.850	α_1	4.616	0.1223	51.38
	α_2	4.012	0.7704	8.16
	α_3	0.997	1.4932	4.21
0.860	α_1	5.040	0.1054	59.61
	α_2	4.752	0.6762	9.29
	α_3	2.389	1.3119	4.79
0.870	α_1	5.357	0.0892	70.44
	α_2	5.252	0.5922	10.61
	α_3	3.451	1.1509	5.46
0.890	α_1	5.763	0.0581	108.14
	α_2	5.691	0.4497	13.97
	α_3	4.800	0.8789	7.15
	α_4	1.836	1.2989	4.84
0.920	α_1	8.677	0	
		3.473	0	
	α_2	5.328	0.2846	22.08
	α_3	5.462	0.5659	11.10
	α_4	3.988	0.8385	7.49
	α_4	2.233	1.1060	5.68
	α_5	0.382	1.3746	4.57

TABLE 1. Exact values of the growth rates $\text{Re}(\alpha)$, frequency $\text{Im}(\alpha)$ and period Ω, of the most-unstable modes for varying T_B. The modes α_i are numbered with respect to increasing frequency.

of bifurcation could be linked to the point of existence of a detonability limit. They present numerical simulations which appear to support this claim. However, the calculations are severely hampered by the required resolution necessary to resolve such dissparate behaviour, and by the length of time their calculations were allowed to run. Moreover, the notion of a detonability limit for a one-step Arrhenius reaction is difficult to define. This is not the case for the chain-branching reaction model employed here, which has an effective switch-off mechanism for the chemical reaction when the detonation shock temperature drops to the chain-branching cross-over temperature T_B. In fact, as we will present below, for the present reaction model the relevant bifurcation point in the linear stability diagram $T_B = 0.913$ is shown to lie substantially far away from the actual numerically calculated detonability limit $T_B \approx 0.87$, and the detonability limit postulations of He & Lee (1995) are found not to be appropriate in this case.

The global stability behaviour shown in figure 2 can be understood from a consid-

eration of the plane steady detonation structure described in the previous section. For low values of T_B, the steady detonation structure has a short temperature-sensitive chain-branching induction zone and its behaviour is dominated by the temperature-insensitive recombination zone. Since the recombination reaction has zero activation energy and depends only on the concentration of chain radicals, there is only a weak coupling mechanism between any chemical reaction and the local thermodynamics. As such, the detonation has a tendency to be stable. This situation is akin to that of a one-step Arrhenius reaction with zero-activation energy (Erpenbeck 1965). But as T_B is increased, the length of the temperature-sensitive chain-branching induction zone becomes more dominant and, at the same time, more sensitive to thermodynamic perturbations as a result of the Arrhenius-type chain-branching reaction rate. Consequently there exists a much stronger local feedback mechanism between perturbations in the thermodynamic state and variations in the chemical dynamics. Thus, it is observed that as T_B increases, the detonation becomes unstable initially to a low-frequency one-dimensional perturbation, with additional high-frequency instabilities appearing as T_B increases further. Finally, we note that Short & Dold (1996) have also considered the effect of transverse disturbances on linear detonation stability for increasing T_B.

6. Numerical method

Below, a nonlinear stability investigation is conducted for the behaviour of an unstable one-dimensional detonation wave driven by the model three-step chain-branching reaction (2.4) with the chain-branching cross-over temperature T_B as the bifurcation parameter. This is achieved through a direct numerical simulation of the rescaled Euler equations (2.1)–(2.3) with the rate equations (2.5)–(2.7) by employing a sophisticated adaptive mesh refinement algorithm (Quirk 1996) with an integration scheme based on Roe's linearized Riemann solver (Glaister 1988). The rescaling is taken such that the new non-dimensional unit of length represents the distance between the shock and the point where half the fuel is consumed, i.e. the half-reaction length $L_{1/2}$.

The mesh refinement scheme employs a hierarchical system of mesh patches (Quirk 1991, 1996) which is able to resolve the finest hydrodynamic and chemical scales that appear in the pulsating detonation problem without substantial overheads. In particular, one must be sure to resolve features such as large pressure changes in the lead detonation shock, the evolution of the chain-branching induction zone whose length can change by upwards of 20-fold, the chain-branching reaction structure and any transient internal gasdynamic or chemical structures, e.g. expansion waves, compression waves, or for higher values of T_B, internal reaction shock waves. For the computations presented below, the computational domain was typically discretized using a uniform mesh of some 8000 cells. Three extra grid levels, each with a refinement factor of 4, were then used to resolve the fine structure of the detonation wave. Thus the effective resolution of the computational grid was that of a uniform mesh of 512 000 cells. Refinement was employed so as to track the main features of the detonation structure independently of one another. All computations were performed using a CFL number of 0.5. Thus a uniform mesh computation would require of the order of 10^{12} cell updates for a complete simulation.

Although at first such resolution might seem excessive, we will present below a number of grid convergence studies which demonstrate the dangers of drawing conclusions from under-resolved calculations in relation to nonlinear dynamic stability

behaviour, particularly with higher values of T_B. Moreover we note that for the flow solver used here, one might expect one cell update to take around 10 μs on a Cray Y-MP class machine, in which case the equivalent uniform mesh simulation would take around 121 days. Alternatively, with the refinement scheme we achieve almost a 400-fold saving in computational effort and can perform a simulation in under a day using just a high-end workstation. These figures are presented merely to impart the sheer scale of the present computations and are not to be taken as exact performance indicators. Nevertheless, they illustrate the prohibitive expense of performing brute force computations even though the present study is only one-dimensional.

In order to obtain the numerical solutions, the governing equations are cast in conservation form and integrated using time operator splitting (Strang 1968). Thus we alternate between updating the flow solution with the chemical source terms switched off and updating the flow solution with the convective terms switched off. For the convective step we have used a Roe-type scheme formulated for an arbitrary equation of state (Glaister 1988). The only part of this scheme that is application dependent is the computation of various partial derivatives in pressure. Given the present equation of state, see (2.3) and (2.7), $p = p(\rho, e, f, y)$ and the required partial derivatives are

$$\left.\begin{array}{ll} \dfrac{\partial p}{\partial \rho} = (\gamma - 1)(e - Qf - (Q + R)y), & \dfrac{\partial p}{\partial e} = (\gamma - 1)\rho, \\[3mm] \dfrac{\partial p}{\partial f} = -(\gamma - 1)\rho Q, & \dfrac{\partial p}{\partial y} = -(\gamma - 1)\rho(Q + R). \end{array}\right\} \quad (6.1)$$

The other operator in our split scheme effectively requires us to integrate (2.5) where the substantive derivative had been replaced by just the time partial derivative. This step is carried out using a two-step Runge–Kutta scheme.

The simulations were started with the steady travelling wave solutions found in §3 and were run at several mesh resolutions (equivalent to 80, 100, 160 and 320 mesh points in the half-reaction length) to allow us to determine the grid sensitivity of the numerical results. As a practical point, we grafted a pre-smeared shock onto the initial steady travelling wave in order to eliminate the start-up errors that are endemic to all shock-capturing schemes. These start-up errors manifest themselves as a pair of low-frequency waves moving on the supposedly passive characteristics (Quirk 1991), and constitute a large-amplitude disturbance to the detonation wave. Therefore, by removing them we ensured that the initial perturbations to the wave were generated by the very much smaller amplitude disturbances arising from the truncation error of our integration scheme. However, our studies also indicate that for a sufficiently well-resolved initial profile, the start-up error has a negligible effect. On the other hand, for under-resolved calculations, say less than 10 cells in the half-reaction length, this is not so and a shock-fitting methodology would be expected to provide better results. For the present study, the travelling waves were propagated upwards of 1000 half-reaction lengths, substantially further than any detonation simulation presented previously, so as to be sure that their nonlinear dynamical behaviour was as fully established as possible.

7. Results

Below we present results which describe the nonlinear pulsating instability of the detonation front which arises by varying the chain-branching cross-over temperature T_B in the model chain-branching reaction scheme (2.4), holding the following other

parameters fixed: $Q = 3$, $R = 0$, $\epsilon_I = 1/20$, $\epsilon_B = 1/8$, $T_I = 3$, $\gamma = 1.2$, $d = 1.2$. These representative parameters correspond to those used in the linear stability analysis presented in §5. Unless noted otherwise, the computations in this section were performed using an effective grid resolution of 160 points in the half-reaction length ($L_{1/2}$) and are all grid converged in behaviour, i.e. further increases in grid resolution have no effect other than to cause small changes in the amplitude and period of the instability.

7.1. *Stable detonation:* $T_B = 0.79$

For $T_B = 0.79$, the steady detonation profile is dominated by a temperature-independent recombination zone with a short chain-branching induction region (figure 1). The linear stability analysis predicts that the steady detonation is stable to small perturbations with the least-stable eigenvalue α_1 having a decay rate $\mathrm{Re}(\alpha_1) = -0.02572$ and a long period of oscillation $\Omega_1 = 24.93$. The next least-stable eigenvalue α_2 has a much shorter period ($\Omega_2 = 3.77$) with a faster decay rate $\mathrm{Re}(\alpha_2) = -0.09782$. The time-evolution of the detonation shock pressure for $T_B = 0.79$ is shown in figure 3. Figure 3(*a*) shows the early evolution for $t < 80$, while figure 3(*b*) shows the longer time evolution for $t < 250$. The early evolution is characterized by small-amplitude high-frequency oscillations of the detonation front together with an underlying slowly evolving low-frequency oscillation. The high-frequency oscillations have a characteristic period $\Omega \approx 3.8$, which corresponds almost exactly with the high-frequency period of the linear mode α_2. These oscillations have dissipated after a propagation time $t \approx 30$. Thereafter, the dominant behaviour is that of a damped low-frequency oscillation with a period $\Omega \approx 25.0$, again almost identical to the period of the linear mode α_1. This oscillation has an initial amplitude $\approx 2.1\%$ of the initial shock pressure, but at $t = 250$ the amplitude of the oscillation has decayed to within $\approx 0.01\%$ of the initial steady shock pressure. For $T_B = 0.79$, the computations have thus confirmed that the steady detonation wave is stable to small perturbations.

7.2. *Marginally stable detonation:* $T_B = 0.80$

By increasing T_B to 0.8, thereby increasing the length of the chain-branching induction region relative to the length of the chain-recombination region, the linear stability analysis predicts that the steady detonation wave will now only be marginally stable to small perturbations. The least-stable mode α_1 has a very slow rate of decay with $\mathrm{Re}(\alpha_1) = -0.005$, with associated long period of oscillation given by $\Omega_1 = 27.74$. For $T_B = 0.80$, the mode α_2 has a decay rate $\mathrm{Re}(\alpha_2) = -0.058$ and short period $\Omega_2 = 4.29$. The detonation shock pressure history is given in figure 4. High-frequency oscillations of the detonation front again appear initially, having a characteristic period $\Omega \approx 4.3$ corresponding to the period of the linear mode α_2, and decay by a time $t = 45$. Thereafter, the dominant behaviour of the shock front is a very slowly decaying low-frequency oscillation, with a characteristic period $\Omega \approx 27.7$. Again this corresponds almost exactly with the period of the linear mode α_1. After a long propagation time of $t = 500$, the amplitude of the pulsation has decayed to within 0.2% of the initial steady detonation shock pressure. Thus, the high-resolution numerical computations exactly correspond to the behaviour predicted by the linear stability analysis for $T_B = 0.8$.

7.3. *Marginally unstable detonation:* $T_B = 0.805$

By increasing T_B from 0.8 to 0.805, a critical chain-branching induction length is reached at which the detonation becomes linearly unstable through a Hopf bifurcation
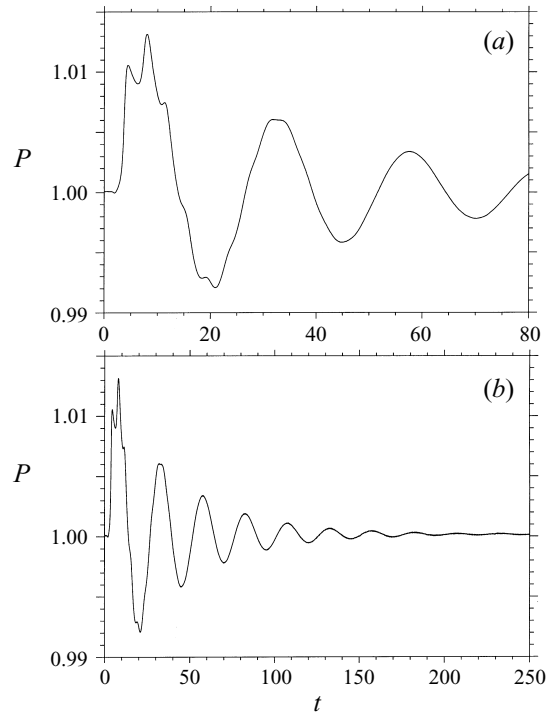
FIGURE 3. Shock pressure history for $T_B = 0.79$. (*a*) Early behaviour shows a fast decay of the high-frequency mode and a slow decay of a low-frequency oscillation. (*b*) Long-time decay of the low-frequency mode.
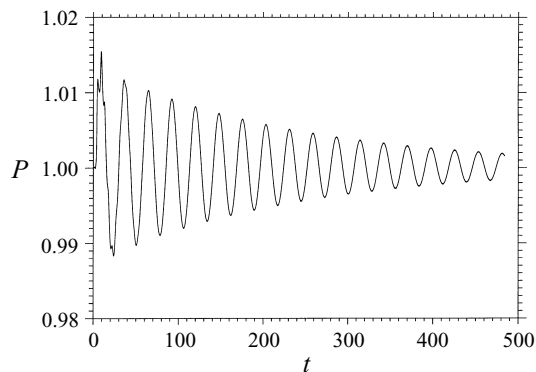

FIGURE 4. Shock pressure history for $T_B = 0.80$ indicating a very slow dissipation of the low-frequency oscillation.

in the low-frequency mode α_1. The mode α_1 is neutrally stable at $T_B = 0.803$. At $T_B = 0.805$, α_1 has a slow growth rate $\mathrm{Re}(\alpha_1) = 0.00355$ with a long period given by $\Omega_1 = 29.31$. At this point the high-frequency oscillatory mode α_2 remains stable with $\mathrm{Re}(\alpha_2) = -0.04147$ and period $\Omega_2 = 4.58$. The detonation shock pressure history is displayed in figure 5. Once more, high-frequency oscillations of the detonation front appear initially, which have a characteristic period of $\Omega \approx 4.6$ and have decayed by $t = 55$. The dominant behaviour is that of the slow amplification of a weakly pulsating instability, exhibiting a low-frequency oscillation of period $\Omega = 29.3$. Again,
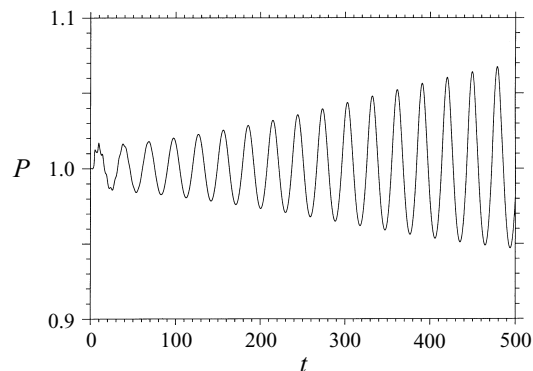
FIGURE 5. Shock pressure history for $T_B = 0.805$ indicating a slow amplification of a low-frequency oscillation.

this agrees almost exactly with the period $\Omega_1 = 29.31$ of the unstable linear mode α_1. After the long propagation time of $t = 400$, the amplitude of the detonation shock pressure oscillation has grown to 10% of the initial steady shock pressure. We remark at this stage on a recent analysis by Bourlioux, Majda & Roytburd (1991*b*) who derived a Landau–Stuart equation which successfully describes the weakly nonlinear growth of a pulsating detonation instability near the neutral stability boundary for a one-step Arrhenius reaction. We believe a similar equation will apply in the present chain-branching reaction model, albeit for modified coefficients in the Landau–Stuart equation.

7.4. *Steady single-period limit-cycle oscillation:* $T_B = 0.82$

For a chain-branching cross-over temperature $T_B = 0.82$, the linear stability analysis predicts the presence of a single unstable oscillatory mode α_1 with growth rate $\mathrm{Re}(\alpha_1) = 0.0235$ and period $\Omega_1 = 34.83$. The high-frequency mode α_2 is still stable having a dissipation rate $\mathrm{Re}(\alpha_2) = -0.0028$ and short period of oscillation $\Omega_2 = 5.55$. Figure 6 shows the detonation shock pressure history for $T_B = 0.82$. For early times, figure 6(*a*) shows the initial excitation of a high-frequency mode with a characteristic period $\Omega = 5.4$, which again dissipates out. The long-term behaviour of the slowly-evolving low-frequency mode is shown in figure 6(*b*). After an evolution time $t = 150$, the detonation shock behaviour is that of a single-mode low-frequency oscillation with constant large amplitude and period. The fully developed oscillation has a maximum pressure peak $P = 1.283 \pm 0.001$ and minimum pressure point $P = 0.876 \pm 0.001$. The pulsation period is given by $\Omega = 35.0 \pm 0.1$. We remark that even though the detonation pulsation is of large amplitude, with a peak approximately 28% of the initial shock pressure, the period $\Omega_1 = 34.83$ of the unstable linear mode α_1 lies remarkably close to the period of the nonlinear pulsation. As noted in Abouseif & Toong (1982), it is possible that the linear stability analysis is detecting the salient features governing the mechanism of the nonlinear pulsation. Finally, we note that the shock pressure history maintains an oscillation with fixed amplitude and period even up to the late time ($t = 600$) that the computation has been conducted. For $T_B = 0.82$, the long-term dynamical behaviour of the detonation shock pressure is that of a steady stable limit cycle with oscillatory period $\Omega = 35.0$ and amplitude $A = 0.407$.

Figure 7 shows two oscillation periods of the late-time pressure history obtained using grids with alternatively 80, 100, 160 and 320 mesh points in the half-reaction
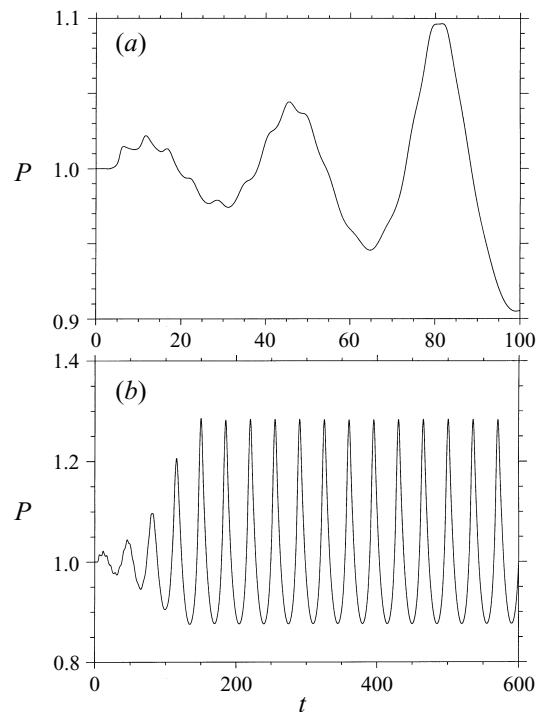
FIGURE 6. Shock pressure history for $T_B = 0.82$. (*a*) Early behaviour shows a decaying high-frequency oscillation with an amplifying low-frequency oscillation. (*b*) The long-time behaviour of the shock front is that of a large-amplitude single-mode pulsating instability with period $\Omega = 35.0$ and amplitude $A = 0.407$.

length. The same basic behaviour is obtained in each case, i.e. the detonation shock pressure evolves as a pulsating limit-cycle instability with constant amplitude and period. The period of the instability is fairly grid insensitive varying from $\Omega = 35.3 \pm 0.1$ on the coarsest grid to $\Omega = 34.9 \pm 0.1$ on the finest grid used for the convergence study. On the other hand, the variation in the amplitude of the pulsation is more marked. We have found that the coarsest grid does not properly resolve the interaction between the detonation front and the finite-amplitude disturbances which arise from within the chain-branching induction zone (described briefly below) and are responsible for the pulsating instability of the front. Thus it overpredicts the maximum amplitude of the pressure pulsation by some 6% compared to that found on the finest grid ($P = 1.358 \pm 0.001$ as against $P = 1.273 \pm 0.001$). As with all the computations presented up to $T_B = 0.85$, an acceptable grid converged solution is obtained with a resolution of 160 mesh points in the half-reaction length.

Although investigated in more detail in a sequel study, we briefly describe the hydrodynamic mechanisms underlying the steady constant-amplitude and frequency pulsating instability for $T_B = 0.82$. At a minimum point in the cycle, the flame zone (where f and y change by $O(1)$ amounts) lies a long distance downstream of the shock. The pressure drop through the flame zone is small, the peak concentration of chain radicals is very low, and the Mach number of the flame in the shock-attached coordinate system is also low. At this point, the detonation has a structure similar to that seen for the larger values of T_B and lower values of k_B in the steady wave (figure 1). Then, a compression wave with finite amplitude and a length
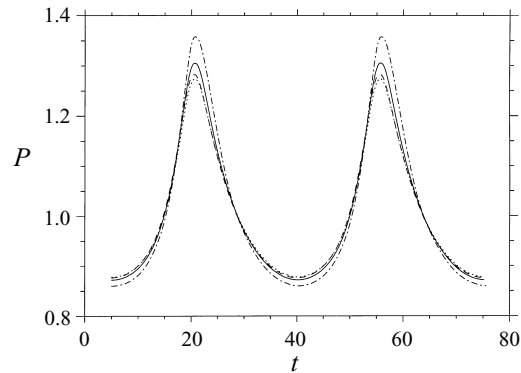
FIGURE 7. A comparison of the amplitudes and frequencies of the fully developed oscillatory instability at $T_B = 0.82$ over two cycles, produced with 80 points$/L_{1/2}(- \cdot -\cdot)$, 100 points$/L_{1/2}$ (——), 160 points$/L_{1/2}$ (– –) and 320 points$/L_{1/2}$ $(\cdots)$. The time scale is shifted such that the first point of the two-cycle oscillation is a minimum of P in the cycle and is set to an arbitrary reference point $t = 5$.
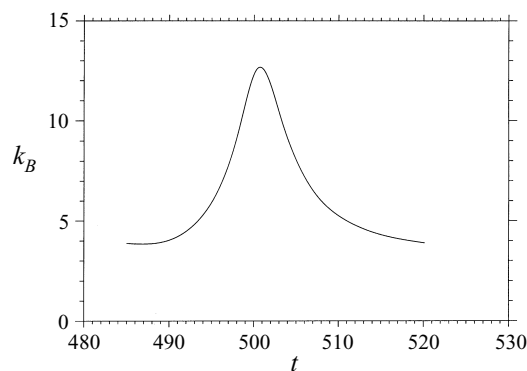

FIGURE 8. Rate constant k_B shock history for $T_B = 0.82$ during a single pulsation of the detonation front.

scale characteristic of the chain-branching induction zone starts to amplify the shock pressure and temperature. The increase in shock temperature drastically increases the chain-branching rate constant k_B and draws the flame zone towards the shock. The peak concentration in chain radicals increases substantially and a substantial pressure drop through the flame zone is observed when the maximum point in the shock-pressure cycle is reached. At this stage, the pulsating detonation has the structure of a steady detonation with a low value of T_B and a higher value of k_B (figure 1). A finite-amplitude expansion wave, again with a length scale characteristic of the chain-branching induction zone, begins to erode the shock, causing the rate constant k_B to decrease and the flame zone recedes from the shock. This process continues until the minimum point in the pressure cycle is again obtained. Figure 8 shows the change in k_B at the shock during a single oscillation. We note that k_B remains well above $k_C = 1$ during the cycle. Thus for $T_B = 0.82$, the steady pulsation is governed by the action of finite-amplitude compression and expansion waves that continuously amplify and erode the shock strength with a constant period.
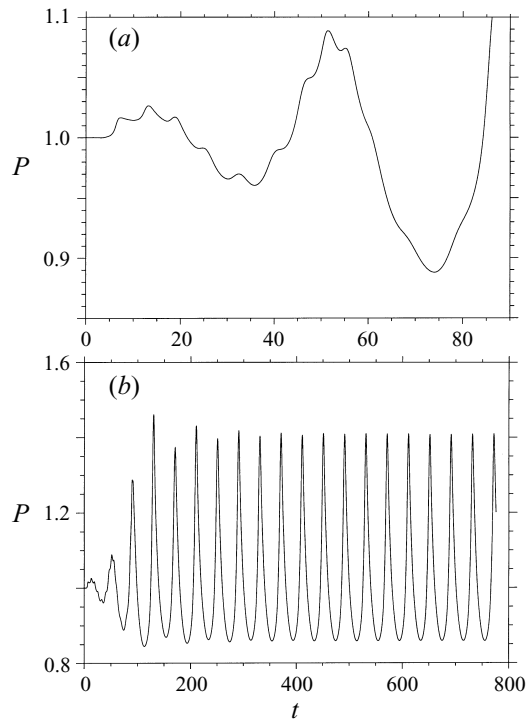
FIGURE 9. Shock pressure history for $T_B = 0.83$. (*a*) Early-time behaviour, and (*b*) long-time behaviour, showing a rapid convergence of initial fluctuations in the shock amplitude to a single-mode limit-cycle with period $\Omega = 40.0$ and amplitude $A = 0.58$.

7.5. *Increasingly less stable limit-cycle oscillation:* $T_B = 0.83$ *to* 0.84

A further increase in the chain-branching induction length of the steady detonation profile as T_B increases from $T_B = 0.82$ leads to a Hopf bifurcation in the previously stable high-frequency mode α_2 at $T_B = 0.821$, and at $T_B = 0.83$ this mode has a positive growth rate $\mathrm{Re}(\alpha_2) = 0.0158$ and period $\Omega_2 = 6.3$. The low-frequency mode α_1 has the larger amplification rate $\mathrm{Re}(\alpha_1) = 0.0332$ and period $\Omega_1 = 39.34$. The detonation shock pressure history for $T_B = 0.83$ is shown in figure 9. Figure 9(*a*) shows, as before, the excitation of high-frequency oscillations with a characteristic period $\Omega = 6.16$ during the initial stages of the propagation, still corresponding almost directly with the period of the linear mode α_2. However, although these modes are now linearly unstable, figure 9(*a*) shows that the high-frequency oscillations are nevertheless not sustained and dissipate after a propagation time $t \approx 100$. For $t > 120$, the detonation shock pressure history shown in figure 9(*b*) indicates the initial presence of a low-frequency two-mode oscillation with the amplitude of the pressure peak of one mode being greater than that of the other mode. However, the amplitude of the larger pressure peak is observed to decay rapidly, while that of the second mode is amplified rapidly. For $t > 500$, the pressure peaks have converged to a value 1.40 ± 0.001. The period of oscillation of the front pulsation for $t > 500$ is given by $\Omega = 40.0 \pm 0.05$. Thus the initial two-mode oscillation decays into a single-mode oscillation of the front. The long-time dynamical behaviour of the detonation again appears to be that of a stable steady single-mode limit-cycle with period $\Omega \approx 40.0$ and amplitude $A = 0.58$. We note the increase in Ω and A over that found for $T_B = 0.82$.
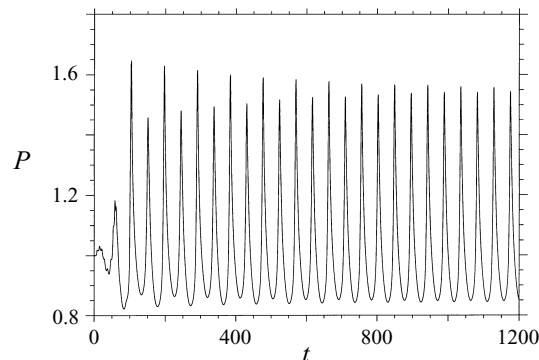
FIGURE 10. Shock pressure history for $T_B = 0.84$, showing a significantly slower decay in the fluctuating shock amplitudes to a long-time attracting single-mode limit cycle with period $\Omega = 46.5$ and amplitude $A = 0.75$.

For $T_B = 0.84$, the stability analysis again predicts the presence of two linearly unstable modes, one low frequency with growth rate $\mathrm{Re}(\alpha_1) = 0.0405$ and period $\Omega_1 = 44.8$ and the other high frequency with a lower amplification rate $\mathrm{Re}(\alpha_2) = 0.0298$ and shorter period $\Omega_2 = 7.2$. Figure 10 shows the detonation shock pressure history for $T_B = 0.84$. Again, high-frequency modes with a characteristic period $\Omega = 6.6$ appear initially, but are observed to dissipate during the initial stages of the propagation. For $t > 75$, a two-mode oscillation of the detonation again emerges initially, with, as for the case $T_B = 0.83$, the value of the pressure peak of one mode being much greater than that of the second mode. Also, both the amplitude of and the difference between the two pressure modes is more pronounced than for $T_B = 0.83$. However, as for $T_B = 0.83$, the amplitude of the larger pressure peak is observed to decay, while that of the second mode is amplified, but at a significantly slower rate than that observed for $T_B = 0.83$. For $t > 900$, the pressure peaks have converged to a value 1.55 ± 0.01. The period of oscillation for $t > 900$ is given by $T = 46.5 \pm 0.1$. Furthermore, by extrapolating the peak pressures past $t = 1200$, we conclude that the amplitudes of the initial two-mode oscillation again converge as the detonation propagates. The long-term dynamical behaviour of the detonation appears to be that of a steady stable single-mode limit-cycle with period $T \approx 46.5$. We also conclude that the single-mode pulsating detonation with constant period found for $T_B \leqslant 0.84$ becomes less stable with increasing T_B. It is apparent that $T_B = 0.84$ is close to the stability boundary of a secondary bifurcation in the periodic limit cycle. On this note, the authors are currently in the process of conducting a Floquet analysis (Drazin & Reid 1981) in order to confirm the stability of the steady limit-cycle oscillation observed for $0.803 < T_B \leqslant 0.84$.

7.6. *Period-doubling bifurcation $T_B = 0.85$*

As T_B is increased from 0.84 to 0.85, a Hopf bifurcation occurs in the previously stable linear mode α_3 at $T_B = 0.844$. At $T_B = 0.85$, this mode has a growth rate $\mathrm{Re}(\alpha_3) = 0.010$ and very short period $\Omega_3 = 4.21$. The low-frequency mode α_1 has a growth rate $\mathrm{Re}(\alpha_1) = 0.0462$ and period $\Omega_1 = 51.38$, while the first high-frequency mode has a growth rate $\mathrm{Re}(\alpha_2) = 0.0401$ and short period $\Omega_2 = 8.16$. Figure 11 shows the early evolution of the detonation shock pressure for $T_B = 0.85$. The first seven high frequency oscillations have a characteristic period $\Omega \approx 8$, while the latter oscillations have a characteristic frequency $\Omega \approx 5$. Although these high-frequency
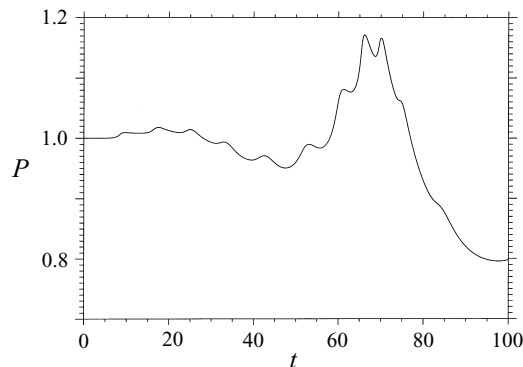
FIGURE 11. Early-time shock pressure history for $T_B = 0.85$.

oscillations are predicted to be linearly unstable, in the nonlinear calculation they dissipate by a time $t \approx 100$.

Figure 12 shows the long-time evolution of the detonation shock pressure for $T_B = 0.85$ as predicted from a computation with two initial effective grid resolutions of (*a*) 160 points/$L_{1/2}$ and (*b*) 320 points/$L_{1/2}$ in the steady detonation wave structure. For the coarser grid, figure 12(*a*) indicates that a secondary period-doubling bifurcation in the steady limit cycle present at $T_B = 0.84$ has occurred and a two-mode oscillation emerges at $T_B = 0.85$. For $t > 1000$, the larger-amplitude pressure modes have a peak value 1.964 ± 0.0005, with trough 0.791 ± 0.0005, while the lower-amplitude pressure modes have a peak value 1.426 ± 0.001 and trough 0.965 ± 0.0005. The period of the oscillations is given by $\Omega \approx 115.3$.

By increasing the resolution to 320 points/$L_{1/2}$ in the initial steady detonation wave structure, however, figure 12(*b*) demonstrates a significant change in the shock pressure history. It is observed that the amplitude of the larger pressure peak decays, while that of the lower-pressure peak increases, but on a very long time scale. By extrapolating the peak and trough pressures of both modes, the long-time behaviour does indicate a decay towards a steady period-doubled oscillation. We calculate a peak pressure for the larger-amplitude mode of 1.71 with trough 0.83, and for the smaller-amplitude mode, a peak pressure of 1.69 with trough 0.84. The period of the two-mode oscillation is given by $\Omega = 112$. We note at this stage the large discrepancies between the period of the linear mode α_1 and the period of the long-time numerically calculated solution. Although, the less-well-resolved calculation has correctly predicted a period-doubled bifurcation, the amplitudes of the cycles are very different from those predicted with the better resolved calculation. We conclude that the calculation with an initial resolution of 160 points in $L_{1/2}$ underestimates the position of the period-doubling bifurcation, hence the larger-amplitude oscillations.

7.7. *Multi-mode pulsation:* $T_B = 0.86$

Figure 13 shows two shock pressure histories for a chain-branching cross-over temperature $T_B = 0.86$ calculated with an initial resolution of (*a*) 80 points and (*b*) 320 points in the half-reaction length. The linear stability analysis shows the presence of the same three unstable modes α_1, α_2 and α_3 found for $T_B = 0.85$. The low-frequency fundamental mode α_1 has a growth rate $\mathrm{Re}(\alpha_1) = 0.0504$ and period $\Omega_1 = 59.61$ at $T_B = 0.86$. The growth rates and periods of the high-frequency modes α_2 and α_3 are given in table 1. The detonation shock pressure history shown in figure 13(*a*)
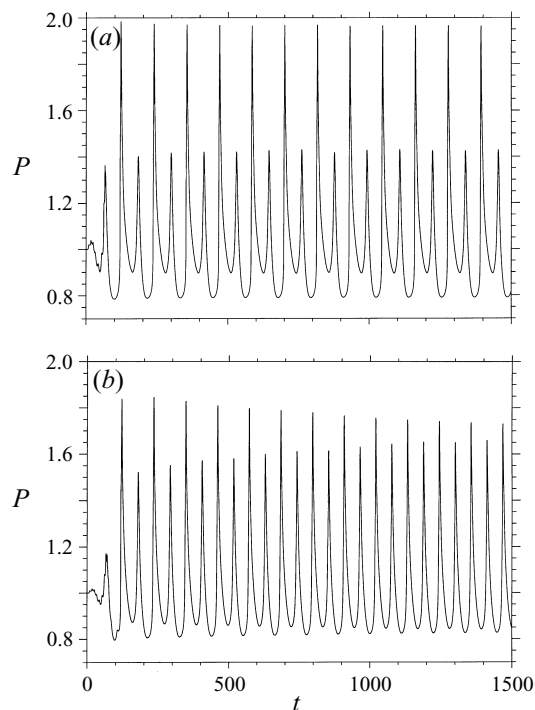
FIGURE 12. Shock pressure history for $T_B = 0.85$ calculated with (*a*) 160 points$/L_{1/2}$ and (*b*) 320 points$/L_{1/2}$. (*a*) A secondary bifurcation to a stable two-mode oscillation is indicated. For the higher-resolution computation, (*b*) indicates the long-term behaviour still to be a period-doubling bifurcation, but with different amplitudes to that seen in (*a*).

displays a highly irregular structure, with a number of pulsating modes of different amplitudes appearing. In particular, we note the presence of several discontinuous large-amplitude pressure rises not previously observed for $T_B < 0.86$. As explained in more detail below, these discontinuous pressure rises occur when a secondary detonation is formed behind the lead detonation shock and runs into the lead shock. Even with the moderately high resolution of 80 points in the half-reaction length, the mesh refinement is not sufficient to properly resolve the appearance of the secondary detonation, nor resolve the shock–shock interaction which occurs when this detonation runs into the lead shock. This results in the highly irregular behaviour observed.

The shock pressure history calculated with 320 points in the half-reaction length illustrates a substantially more regular pulsating oscillation of the front, although over the time scale of the calculation conducted the oscillations do have a multi-mode character. A much extended calculation than that possible here would be needed to established the long-term behaviour, and to determine whether the solution is indeed chaotic or has simply undergone a series of further period-doubling bifurcations. The initial seven high-frequency pulsations of the front have a characteristic frequency $\Omega = 9.1$ with the latter two having a frequency $\Omega = 4$. The shock pressure initially rises to a value $P = 1.36$, before decaying and giving rise to a period of nearly uniform shock pressure for $100 < t < 149$. These periods of uniform shock pressure have not been observed previously for $T_B < 0.86$.

In a sequel, we will show that these regions of uniform shock pressure entail a
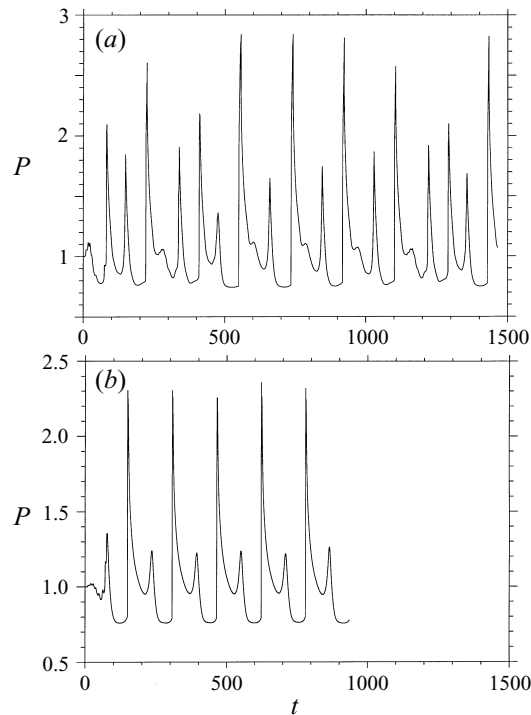
FIGURE 13. Shock pressure history for $T_B = 0.86$ calculated with (*a*) 80 points/$L_{1/2}$ and (*b*) 320 points/$L_{1/2}$. The computation shown in (*a*) illustrates a highly irregular behaviour of the detonation shock front, arising from the failure to satisfactorily resolve the appearance of internal shock waves in the detonation structure on the coarser grid. The resolved computation shown in (*b*) indicates the shock front pressure has undergone a bifurcation to a multi-mode chaotic oscillation. The large-amplitude pressure modes arise as a result of an internal reaction shock collision with the detonation front, while the lower-amplitude modes result from the interaction of finite-amplitude compression and expansion waves with the detonation shock front.

decoupling between the detonation shock and reaction zone, where the detonation structure consists of a long chain-branching induction zone and the reaction zone assumes the form of a low-Mach-number fast flame. A finite-amplitude compression wave is then seen to run ahead of the reaction zone, which steepens into a shock wave and combines with the reaction zone to form a secondary detonation behind the lead shock. At $t = 149$, a large discontinuous shock pressure rise occurs when the secondary detonation collides with the lead shock. The shock pressure increases to $P = 2.31$, nearly two and a half times larger than the steady detonation shock pressure. Subsequently, we note first a decay in the shock pressure to $P = 2.04$ followed by a rise to $P = 2.25$, caused by the ignition of material in front of the contact surface generated by the detonation-shock interaction. Thereafter, the shock pressure decays rapidly until at $t = 211$ a small-amplitude continuous oscillation occurs. At $t = 260$, a uniform period again results, and the cycle of events as described above is repeated for the further five large-amplitude rises shown. The peak amplitudes of the shock pressure reached in each further oscillation are given by $P = 2.31$, $P = 2.25$, $P = 2.37$ and $P = 2.32$ respectively.

Figure 14 shows the change in k_B at the shock during the large-amplitude pressure oscillation. During the regions of constant shock pressure, the rate constant drops to the value $k_B = 1.6$, which is just above the chain-branching rate constant $k_C = 1$. Sub-
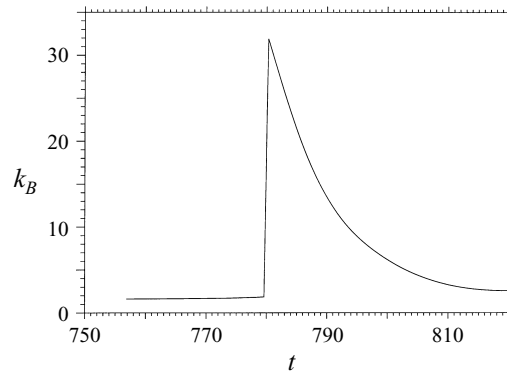
FIGURE 14. Rate constant k_B shock history for $T_B = 0.86$ during a large-amplitude pressure pulsation of the detonation front.
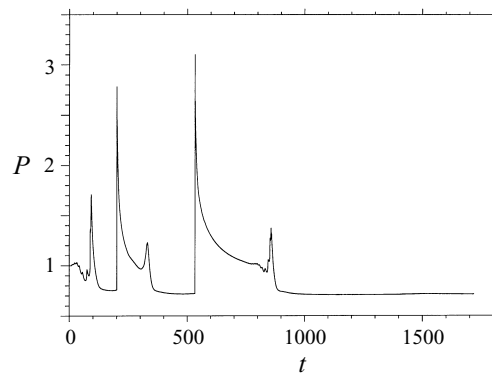

FIGURE 15. Shock pressure history for $T_B = 0.87$, displaying two long regions of constant low shock pressure. The latter indicates detonation failure.

sequently, k_B jumps sharply to 31.9 after shock collision. Thus for $T_B = 0.86$, we have demonstrated a remarkably different shock pressure history trace to that observed previously. In particular, the hydrodynamical mechanisms governing the pulsating instability are now highly complex, involving a decoupling of the detonation shock and reaction zone, followed by the subsequent formation of secondary detonation waves.

7.8. *Detonability limit: $T_B = 0.87$*

Figure 15 shows the shock pressure history calculated for $T_B = 0.87$. For this value of T_B, it can be seen from figure 1 that the steady detonation possesses a chain-branching induction length and chain-recombination region which are now of comparable order in length. The linear stability analysis reveals that the steady detonation structure is still unstable to the same three oscillatory modes identified for $T_B = 0.86$. The fundamental low-frequency mode α_1 now has a growth rate $\mathrm{Re}(\alpha_1) = 0.0536$ and period $\Omega_1 = 70.44$. The modes α_2 and α_3 have amplification rates $\mathrm{Re}(\alpha_2) = 0.0525$ and $\mathrm{Re}(\alpha_3) = 0.0345$ with periods $\Omega_2 = 10.61$ and $\Omega_3 = 5.46$ respectively. We note the similar amplification rates of the low-frequency mode α_1 and high-frequency mode α_2.

The shock pressure history shows the initial presence of six high-frequency oscillations of the front with a characteristic period $\Omega = 11.7$. We note, however, that

despite the initial similarity in growth rates between the linear modes α_1 and α_2, the high-frequency modes dissipate out, as is the case for all previous values of T_B. A moderately large, but continuous, jump in shock pressure occurs at $t \approx 85.0$, taking the pressure amplitude to $P = 1.71$. The shock pressure is then seen to decay rapidly and a region of almost uniform shock pressure, where $P \approx 0.75$, ensues for $130 < t < 205$. At $t = 205$, a first discontinuous jump in the shock pressure occurs, taking the pressure to $P = 2.78$. Once again, the shock pressure decays rapidly, and gives rise to a small pressure oscillation at $t = 305$, in a fashion observed previously for $T_B = 0.86$. Between $t = 350$ and $t = 533$ a long region of quiescent shock pressure is seen where $P = 0.72$, which is over twice as long as the first region of uniform shock pressure. At $t = 533$, a substantial, discontinuous jump in the shock pressure again occurs, rising to a maximum $P = 3.11$. At this point, the shock pressure first decays rapidly before the rate of decay is slowed. At $t = 750$, when $P = 1.01$, high-frequency oscillations of the shock front are again observed. Interestingly, the characteristic period of these oscillations is $\Omega = 11.7$. Following these small-period oscillations, a low-amplitude pulsation of the front results. For $t > 900$, the shock pressure again equilibriates and between $t = 900$ and $t = 1720$ has a value $P = 0.713$. At the termination of the simulation, a third large pressure rise event has not yet appeared, and the detonation has effectively failed. Thus, we propose that at $T_B = 0.87$ the detonability limit has been reached. The reasons for this are explored below.

Corresponding to the shock pressure $P = 0.713$ found during the latter stages of quiescent shock propagation, the shock temperature is given by $T = 0.873$. This is only barely above the chain-branching cross-over temperature $T_B = 0.87$, and as such, has a profound implication for the rate of radical production behind the shock. As we have previously demonstrated in §4, when the shock temperature drops to very close to the relevant chain-branching cross-over temperature, the concentration of chain radicals can only grow at the exponentially small rate k_I^{-1} and the reaction zone drops an exponentially large distance behind the shock. Thus, a complete decoupling between the reaction zone and shock occurs and the detonation quenches. The mechanisms behind the quenching will be explored in more detail in a sequel, but are essentially as described above.

7.9. *Rapid quenching:* $T_B \geqslant 0.87$

Figures 16(*a*) and 16(*b*) show respectively the early- and long-time pressure trace history associated with a chain-branching cross-over temperature of $T_B = 0.89$, in which a rapid quenching of the detonation occurs. The linear stability analysis now predicts the presence of four unstable oscillatory modes, with again the largest amplification rate being associated with the low-frequency mode α_1 with $\text{Re}(\alpha_1) = 0.0576$ and $\Omega_1 = 108.14$. The growth rates and periods of the other three high-frequency modes are shown in table 1. Figure 16(*a*) shows that even at this large value of T_B, where the reaction zone in the steady detonation profile lies increasingly far back from the shock, the initial history is characterized by several high-frequency oscillations of the front with an average period $\Omega = 12.5$, which ultimately decay out.

Figure 16(*b*) shows the quenching sequence of the detonation for $T_B = 0.89$. After the initial rise in pressure from $t = 0$, the shock decays rapidly. At $t = 180$, there is a small pressure oscillation, which takes the shock pressure to a value $P = 0.783$, before decaying down to a value $P = 0.700$. The shock pressure then remains at this value until the simulation is terminated at $t = 2000$, and the detonation is quenched. The shock temperature corresponding to $P = 0.700$ is $T = 0.884$, which in this case
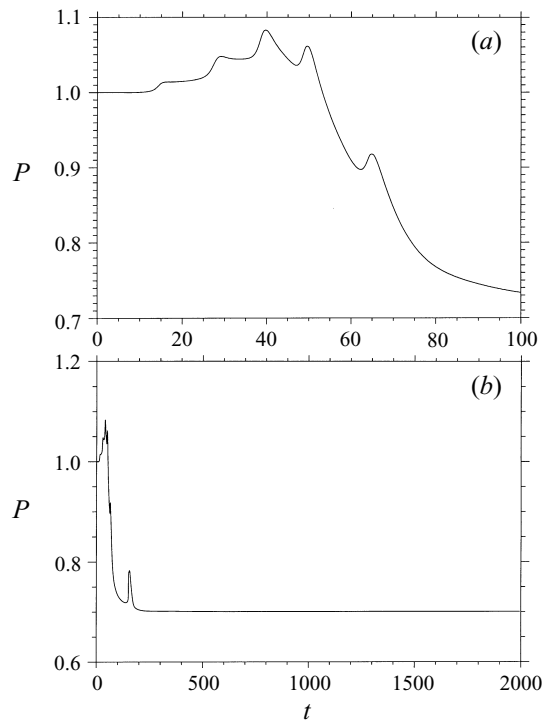
FIGURE 16. Shock pressure history for $T_B = 0.89$. (*a*) Early behaviour shows the appearance and decay of high-frequency oscillations as the shock pressure falls quickly. (*b*) The failure of the detonation wave as the detonation shock temperature drops to the chain-branching cross-over temperature $T_B = 0.89$.
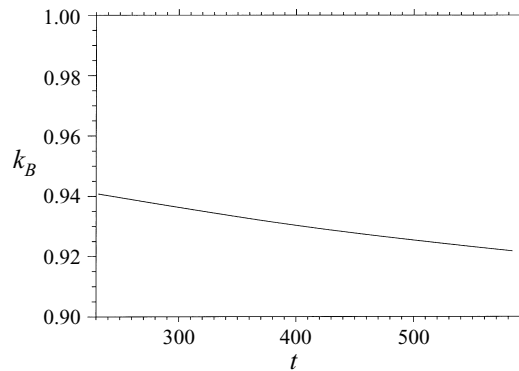

FIGURE 17. Rate constant k_B shock history for $T_B = 0.89$ during quenching.

is almost precisely equal to, but below, the chain-branching cross-over temperature of $T_B = 0.89$. As explained above, when such a situation arises the concentration of chain carriers can only grow at the exponentially small rate k_I^{-1}, and the reaction zone drops an exponentially large distance behind the shock. Since the energy of chemical reaction arising from within the reaction zone structure is required to drive the detonation, then the detonation has effectively quenched. Figure 17 shows the value of k_B at the shock during the quenching.
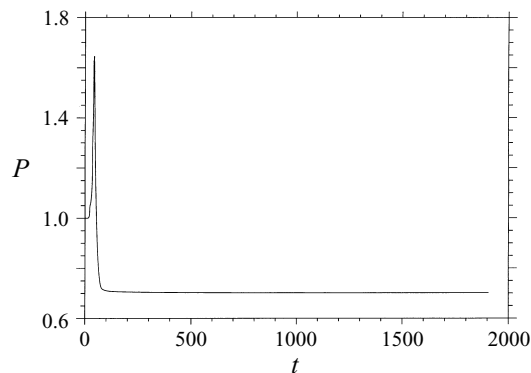
Figure 18. Shock pressure history for $T_B = 0.92$.

We also note here an essential difference between the present quenching scenarios observed for $T_B > 0.87$ using a chain-branching reaction model, and a one-step Arrhenius thermal decomposition model. For the three-step reaction model here, we can established a definition for the detonability limit, i.e.

the detonability limit occurs when the detonation shock temperature drops to the chain-branching cross-over temperature.

The nature of the chain-branching reaction is such as to act like a chemical switch: if the detonation shock temperature drops to the chain-branching cross-over temperature, the chain-branching reaction is effectively switched off. In contrast, there is no clear definition for what one would choose for the detonability limit of a detonation driven by a one-step Arrhenius chemical reaction.

Figure 18 shows the shock pressure history for a detonation with $T_B = 0.92$. For this value of T_B we are entering a regime where the chain-branching induction length is now longer than the chain-recombination zone. In a similar manner to that observed for $T_B = 0.87$ and $T_B = 0.89$, the detonation wave ultimately quenches, as the shock temperature this time drops below that of the chain-branching cross-over temperature $T_B = 0.92$ to $T = 0.885$. On passing the barrier of the cross-over temperature, the detonation then effectively fails via the mechanisms described above. As noted earlier, this case is also of interest in relation to the results of the present linear stability analysis, to the studies of He & Lee (1995) and Short (1997) and to the earlier analysis of Buckmaster (1988). As T_B increases through 0.913, the low-frequency oscillatory linear mode α_1 undergoes a pitchfork bifurcation and splits into a slowly evolving low-frequency non-oscillatory root and a faster-evolving non-oscillatory root.

Buckmaster (1988) has shown that the presence of a slowly evolving non-oscillatory mode in a detonation reacting with one-step Arrhenius kinetics with a high-activation energy leads to large transient pressure increases at the detonation shock. It is also found that as the pressure increases, the effect of the chemical reaction term in the energy balance equation diminishes and the detonation shock is unable to sustain the large increases in pressure and ultimately decays. This is precisely the early behaviour observed in figure 18. For the pressure traces observed for $T_B < 0.92$, there is at least initially some low-frequency small-amplitude oscillation of the detonation front, before large pressure rises ensue. However, for $T_B = 0.92$, it is observed that the detonation shock pressure increases both rapidly and monotonically from $P = 1$ and reaches $P = 1.645$ at a time $t = 40$. The shock then decays rapidly down to $P = 0.7011$ for $t > 100$. Thus the behaviour in shock pressure predicted by Buckmaster (1988)

when a low-frequency non-oscillatory root is present for one-step Arrhenius kinetics with a large activation energy is also repeated for the present chain-branching reaction model. We also observe that the definition of the detonability limit as the bifurcation point between oscillatory and non-oscillatory modes in the linear stability diagram, given by He & Lee (1995), is shown to be inappropriate for the present reaction model. Here, the linear bifurcation point occurs for $T_B = 0.913$, while the detonability limit is reached at $T_B = 0.87$.

Before concluding, it remains to make one further point regarding the mechanism behind one-dimensional detonation failure observed for $T_B \geqslant 0.87$. Lee (1991), with further comments by He & Lee (1995), suggests that by removing the transverse wave structure in a multi-dimensional detonation, the resulting quasi-one-dimensional detonation structure will always fail. The work presented here offers a different conclusion. For the present model reaction scheme, if the chain-branching cross-over temperature is sufficiently high it is possible that during the oscillation of the detonation front, the decay of the front can reduce the detonation shock temperature to the chain-branching cross-over temperature. The reaction is then effectively switched off and the detonation fails. Thus if the detonation is to propagate for such cross-over temperatures, a transverse wave structure would be necessary to locally raise the shock temperature above the cross-over temperature in order that reaction can proceed at a finite rate. However, if the cross-over temperature for the reaction is sufficiently low, the existence of quasi-one-dimensional oscillatory detonation structure cannot be ruled out.

8. Summary

We have examined both the linear stability and the nonlinearly unstable large-amplitude pulsating behaviour of a one-dimensional wave driven by a model three-step chain-branching reaction. With this model chemical scheme, which is the simplest realistic mechanism able to reproduce the reaction dynamics of an actual chain-branching reaction, the steady detonation structure consists of a temperature-sensitive chain-branching induction region, a main reaction zone and a temperature-insensitive recombination region. The ratio of the length of the chain-branching induction zone to recombination zone is controlled by T_B, the chain-branching cross-over temperature at which the chain-branching and recombination reaction rates are equal. The linear stability analysis predicts that those detonation waves with sufficiently low T_B, whose structure is dominated by the chain-recombination reaction, have a tendency to be stable to small perturbations. By increasing T_B and increasing the length of the chain-branching induction region relative to the chain-recombination zone, the detonation becomes linearly unstable, with the most unstable root always being a low-frequency mode. The numerical computations demonstrate that for a wide range of $T_B > 0.803$, the long-time nonlinear dynamical behaviour of the detonation shock front is that of a single-period large-amplitude stable limit-cycle with a low-frequency of oscillation. As T_B is increased in this range, the amplitude and period of the limit cycle both increase. This corresponds to an increasingly lower value of the chain-branching rate constant k_B in the steady detonation profile at the detonation shock. Also, in this regime, the periods of the pulsation agree well with the period of the low-frequency unstable eigenvalue identified in the linear stability analysis, indicating that the linear theory contains the salient physical processes sustaining the pulsating oscillations.

At $T_B \approx 0.85$, a period-doubling bifurcation is seen to have occurred giving a two-mode pulsation in the detonation shock pressure. At $T_B = 0.86$, a multi-mode

oscillation is observed, which contains large discontinuous jumps in the detonation shock pressure caused by its interaction with a secondary detonation formed behind the lead shock. For $T_B > 0.87$, the detonation shock temperature drops close to the chain-branching cross-over temperature, and the chain-branching rate constant at the shock is close to the chain-recombination rate constant. Chain radicals can only then grow at an exponentially small rate and the chain-branching induction length becomes exponentially large. In such circumstances, we conclude that the detonation has failed, and the detonability limit has been reached. Moreover, the chemical switch-off mechanism found in the three-step chain-branching reaction model that causes this quenching to occur is not present for one-step Arrhenius reaction kinetics.

We also introduce a sophisticated adaptive mesh refinement strategy (Quirk 1991, 1996) for solving the pulsating detonation problem. While the present grid resolutions might appear excessive compared to previous numerical studies of pulsating detonations (e.g. Bourlioux *et al.* 1991*a*), we demonstrate that under-resolved calculations will give erroneous predictions of the shock pressure history. Moreover, we conclude that algorithmic arguments such as whether to track or capture shocks are irrelevant if the computational grid is too coarse to resolve the smooth but small-scale structures appearing within the detonation wave. For example, with the present reaction model, we feel it is more important to resolve the radical spike accurately as this directly affects the release of chemical energy into the detonation and so ultimately dictates the grid resolution required for a reliable simulation.

In conclusion, the work presented here is the first comprehensive study of the propagation of unstable one-dimensional pulsating detonation waves for a reaction model other than that of a one-step Arrhenius chemical rate model, which is based on a linear stability analysis. The model three-step reaction is able to reproduce the essential dynamics of a real chain-branching reaction model and is the first stage on the road to a comprehensive understanding of the behaviour of detonations in real reactive materials.

REFERENCES

ABOUSEIF, G. & TOONG, T. Y. 1982 Theory of unstable one-dimensional detonations. *Combust. Flame* **45**, 64–94.

ALPERT, R. L. & TOONG, T. Y. 1972 Periodicity in exothermic hypersonic flows about blunt projectiles. *Acta Astron.* **17**, 538–560.

BOURLIOUX, A., MAJDA, A. J. & ROYTBURD, V. 1991*a* Theoretical and numerical structure for unstable one-dimensional detonations. *SIAM J. Appl. Maths* **51**, 303–343.

BOURLIOUX, A., MAJDA, A. J. & ROYTBURD, V. 1991*b* Nonlinear development of low-frequency one-dimensional instabilities. In *Dynamical Issues in Combustion Theory* (ed. P. Fife, A. Linan & F. Williams). IMA Volumes in Mathematics and its Applications, vol. 35, pp. 63–83. Springer.

BUCKMASTER, J. D. 1988 Pressure transients and the genesis of transverse shocks in unstable detonations. *Combust. Sci. Tech.* **61**, 1–20.

DOLD, J. W. & KAPILA, A. K. 1991 Comparison between shock initiation of detonation using thermally-sensitive and chain-branching chemical models. *Combust. Flame* **85**, 185–194.

DRAZIN, P. G. & REID, P. E. 1981 *Hydrodynamic Instability*. Cambridge University Press.

ERPENBECK, J. J. 1962 Stability of steady-state equilibrium detonations. *Phys. Fluids* **5**, 604–614.

ERPENBECK, J. J. 1964 Stability of idealized one-reaction detonations. *Phys. Fluids* **7**, 684–696.

ERPENBECK, J. J. 1965 Stability of idealized one-reaction detonations: zero activation energy. *Phys. Fluids* **8**, 1192–1193.

FICKETT, W. & DAVIS, W. C. 1979 *Detonation.* University of California Press.

FICKETT, W., JACOBSON, J. D. & SCHOTT, G. L. 1972 Calculated pulsating one-dimensional detonations with induction-zone kinetics. *AIAA J.* **10**, 514–516.

FICKETT, W. & WOOD, W. W. 1964 Flow calculations for pulsating one-dimensional detonations. *Phys. Fluids* **9**, 903–916.

GLAISTER, P. 1988 An approximate linearized Riemann solver for the Euler equations for real gases. *J. Comput. Phys.* **74**, 382–408.

GRAY, B. F. & YANG, C. H. 1965 On the unification of the thermal and chain theories of explosion limits. *J. Phys. Chem.* **69**, 2747–2750.

GRIFFITHS, J. F. & BARNARD, J. A. 1995 *Flame and Combustion.* Blackie Academic & Professional.

HE, L. & LEE, J. H. S. 1995 The dynamical limit of one-dimensional detonations. *Phys. Fluids* A **7**, 1151–1158.

KAPILA, A. K. 1978 Homogeneous branched-chain reactions: Initiation to completion. *J. Engng Maths* **12**, 221–235.

LEE, J. H. S. 1984 Dynamic parameters of gaseous detonations. *Ann. Rev. Fluid Mech.* **16**, 311–336.

LEE, J. H. S. 1991 Dynamic structure of gaseous detonation. In *Dynamic Structure of Detonation In Gaseous and Dispersed Media* (ed A. A. Borissov), pp 109–141. Kluwer.

LEE, H. I. & STEWART, D. S. 1990 Calculation of linear instability: one-dimensional instability of plane detonation. *J. Fluid Mech.* **216**, 103–132.

McVEY, J. B. & TOONG, T. Y. 1971 Mechanism of instabilities of exothermic hypersonic blunt-body flows. *Combust. Sci. Tech.* **3**, 63–76.

QUIRK, J. J. 1991 An adaptive grid algorithm for computational shock hydrodynamics. PhD thesis, Cranfield Institute of Technology, UK.

QUIRK, J. J. 1996 A parallel adaptive mesh refinement algorithm for computational shock hydrodynamics. *Appl. Numer Maths* **20**, 427–453.

SHORT, M. 1997 Multi-dimensional linear stability of a detonation wave at high-activation energy. *SIAM J. Appl. Maths* **57**, 306–326.

SHORT, M. & CLARKE, J. F. 1997 Linear stability of a fast-flame, in preparation.

SHORT, M. & DOLD, J. W. 1996 Multi-dimensional linear stability of a detonation wave with a model three-step chain-branching reaction. *Math. Comput. Model.* **24**, 115–123.

STRANG, G. 1968 On the construction and comparison of finite-difference schemes. *SIAM J. Numer. Anal.* **5**, 506–517.

STREHLOW, R. A. 1970 Multi-dimensional detonation wave structure. *Astro. Acta* **15**, 345–357.

STREHLOW, R. A. 1986 *Combustion Fundamentals.* McGraw-Hill.

WILLIAMS, F. A. 1985 *Combustion Theory.* Addison-Wesley.